Multiple fragmentation of atoms in femtosecond laser pulses

A Becker[1], **R Dörner**[2] **and R Moshammer**[3]

[1] Max-Planck-Institut für Physik komplexer Systeme, Nöthnitzer Str. 38, 01187 Dresden, Germany
[2] Institut für Kernphysik, Max-von-Laue Str. 1, 60438 Frankfurt, Germany
[3] Max-Planck-Institut für Kernphysik, Saupfercheckweg 1, 69117 Heidelberg, Germany

E-mail: abecker@mpipks-dresden.mpg.de, doerner@atom.uni-frankfurt.de and moshamme@mpi-hd.mpg.de

Abstract
Multiple ionization of atoms by an ultrashort intense laser pulse is a process in which the few-body problem is closely interrelated with the highly nonlinear interaction between the electrons and the external field. We review recent advances in unveiling the mechanisms behind the unusually large ion yields for double and multiple ionization observed in a strong laser pulse. Its study requires on one hand the combination of highly differential experimental techniques with laser systems having high repetition rates and on the other the development of new theoretical methods to simultaneously account for the long-ranged Coulomb interaction between the particles and the field nonlinearity. Different mechanisms are analysed diagrammatically and quantitatively in comparison with experimental data for the total ion yields. Distributions for the electron and ion momenta of coincidence measurements are discussed along with predictions of the various theoretical methods.

1. Introduction

About 25 years after the quantum mechanical description of the photo-electric effect by Einstein [1], it was Göppert-Mayer [2] who predicted that the energies of more than one photon can be combined to achieve the emission of an electron from an atom or molecule, when the energy of one photon is not sufficient to overcome the binding potential. The observation of such multiphoton phenomena requires a high photon density at the location of the target, which became available with the evolution of the laser in the 1960s. Modern laser systems (e.g. the Ti:sapphire lasers) provide peak light intensities of the order of 10^{20} W cm^{-2} or above in pulses shorter than 100 fs. The field strength at these intensities is

a hundred times the Coulomb field binding the ground state electron in the hydrogen atom[4]. These extreme photon densities allow highly nonlinear multiphoton processes such as above-threshold ionization, high harmonic generation, laser-induced tunnelling, Coulomb explosion, multiple ionization and others, where up to a few hundred photons can be absorbed from the laser field.

Single ionization and other single-active-electron phenomena in intense fields have been intensively studied for many years. The experimental observables are the ionization yields as a function of the laser intensity, the energy and angular distribution of the emitted electron or the emission of higher harmonic light. We refer the interested reader to several review articles covering this broad field [3–10].

In this review, we focus on recent advances in unveiling the mechanisms of *double and multiple ionization* in strong laser fields. It reveals new aspects of the electron–electron correlation, different from those in the ground state of atoms or in the double ionization by charged particle (see [11] for a review) or single photon (see [12, 13] for reviews) impact. This few-body problem is not only an intellectual challenge; it also has a wide ranging impact on many fields of science and technology. It is the correlated motion of electrons which is responsible for the structure and the evolution of large parts of our macroscopic world. It drives chemical reactions and is the ultimate reason for superconductivity and many other effects in the condensed phase. In atomic processes, few-body correlation effects can be studied in a particular clear manner.

With the increase of the electron number in the process, the challenges in experimental observations and theoretical analysis increase. In the early experiments, the yields of the multiply charged ions were measured. Recently it has become possible to also detect the energy or the momentum vector of the electrons and the ions in coincidence by combining highly differential experimental techniques that are standard in the fields of ion–atom, electron–atom and high energy single photon–atom collision studies, with laser systems having a kilohertz repetition rate. On the other hand, for an exact *ab initio* simulation of a system with two electrons one needs to solve a set of six-dimensional partial differential equations over a large spacetime grid. Considerable progress has been made recently in this direction using high power computers [14–19]. An alternative *ab initio* approach is provided by the intense-field many-body S-matrix theory (IMST). It is a systematic approximation method for the analysis of processes which require to account simultaneously for different interactions of similar strength (in the present case the Coulombic interaction and the laser interaction). Further, a number of approximative methods have been developed, e.g. lower-dimensional numerical simulations or classical trajectory Monte Carlo calculations. Below, we present and discuss recent observations and their analysis as well as the resulting physical picture of the correlated electron emission from an atom interacting with an intense laser pulse.

2. Mechanisms of double ionization in strong fields

2.1. Ionization yields

Single ionization of atoms and molecules in intense laser pulses can be satisfactorily described using the single-active-electron (SAE) approximation [20], where only the outermost electron, moving in the effective potential of the ionic core and the other electrons, is assumed to interact with the field. In this picture the electron–electron interaction is negligible. It would imply

---

[4] The atomic unit of electric field strength felt by an electron on the first Bohr orbit of the hydrogen atom is $\mathcal{E}_a = e/a_0^2 \simeq 5.1 \times 10^9$ V cm^{-1}, the corresponding intensity being $I_a = 3.51 \times 10^{16}$ W cm^{-2}. It corresponds to about 10^{10} coherent photons in a box of the size of the wavelength of a Ti:sapphire laser (800 nm).
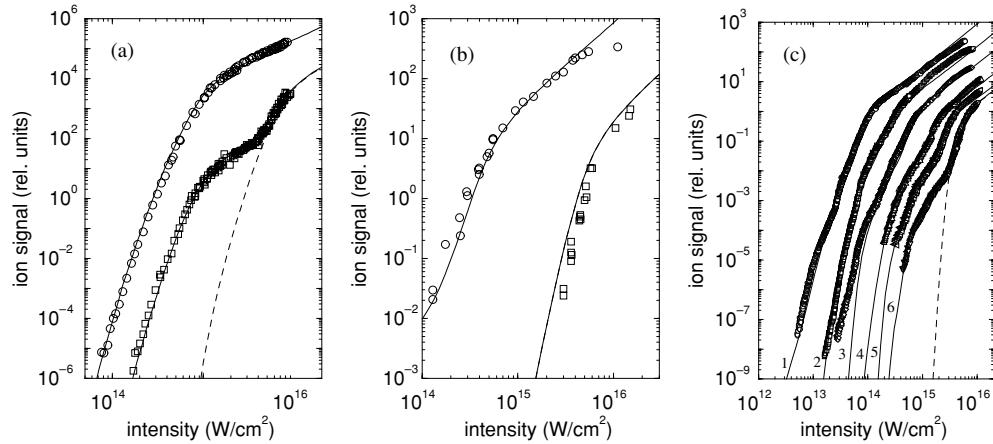
Figure 1. Measured yields of double ionization of helium at 780 nm (panel a, [21]) and 248 nm (panel b, [22]), and multiple ionization of xenon at 800 nm (panel c, [23]) for linearly polarized laser light. Predictions of the *S*-matrix theory [24, 25] are shown as solid lines. Note the strong enhancement of the double and multiple ionization yields over the sequential prediction at the infrared wavelengths (dashed lines) and its absence at 248 nm.

for the double ionization process that the electrons are emitted *sequentially*, i.e. the neutral atom first gets ionized, then the cation is further ionized independently of the first step, etc. But theoretical predictions based on this sequential ionization mechanism do not account for the large double and multiple ionization yields in intense laser fields observed at near infrared wavelengths. This is exemplified in figure 1 in plots of the ionization yields as a function of the laser intensity. Here both double ionization yields of He as observed by Walker *et al* (figure 1(a), [21]) and multiple ionization yields of Xe as measured by Larochelle *et al* (1(c), [23]) are shown. At low intensities, the experimental data show a strong enhancement of the double and multiple ionization yields over the predictions of the sequential mechanism (dashed lines, *S*-matrix calculations [24, 25], or nearly equal results of SAE simulations, see e.g. [21]). There is also the ubiquitous 'knee' structure to be seen in the double (and multiple) ionization curves, which has been observed for the first time in the 1980s by L'Huillier *et al* [26]. Also note that at 248 nm (figure 1(b)) no excessive double ionization yield over the prediction of the sequential mechanism has been observed [22]. Thus, while at near infrared wavelengths a *nonsequential* ejection of two or more electrons dominates, there is no sign of it at the shorter UV wavelength.

2.2. Mechanisms and diagrams

What is the mechanism leading to nonsequential double (and multiple) ionization? This seemingly well-defined question does not necessarily have a unambiguous quantum mechanical answer, since it is not always straightforward to deduce such a picture from a theoretical analysis and even if this is possible often the contributions from different mechanisms have to be added coherently. An example is the single-photon double ionization process at low light intensities. Here at least contributions of two mechanisms, called shake-off and two-step-one (their strong field analogues will be discussed below), have to be considered to obtain an agreement with the observations [27, 28]. This is not the case for nonsequential
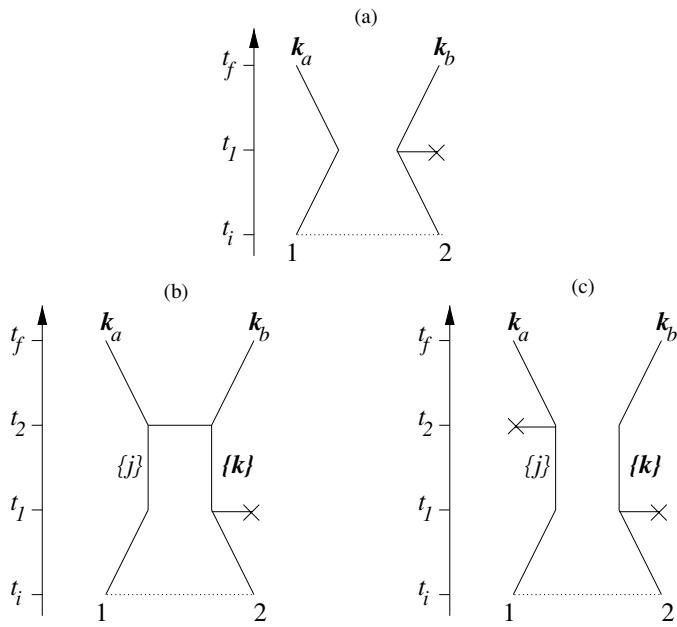
Figure 2. Three (out of eight) diagrams that are generated by the first leading terms of IMST. The diagrams correspond to qualitative mechanisms for nonsequential double ionization proposed in the literature, namely (a) shake-off, (b) rescattering and (c) sequential ionization and collective tunnelling.

double ionization in strong fields. As it will be seen below, there is one mechanism that dominates strongly.

Becker and Faisal have identified [29–31] diagrammatically and quantitatively the main mechanism of double ionization using the IMST. This theory is a thorough rearrangement of the usual S-matrix series such that all features of the process appear in the first leading terms of the series (for a review of IMST see [32]). In the case of double ionization of an atom, the IMST generates eight Feynman-like diagrams up to the second order of the series. Three of these diagrams are shown in figure 2, which is a form of representation of the S-matrix terms, that is convenient to obtain intuitive pictures or mechanisms of the process of interest. In the diagrams time is assumed to flow from the bottom upward and straight lines stand for the evolution of the two electrons. The three diagrams in figure 2 correspond to the following mechanisms qualitatively proposed before in the literature:

Shake-off: if one electron is removed rapidly from an atom or a molecule by the interaction with an intense field, for example, the wavefunction of the remaining electron has to relax to the new eigenstates of the altered potential. Some of these states are in the continuum, so that a second electron can be *shaken off* during this relaxation process. This process corresponds to the first-order diagram in figure 2(a). Here, the two electrons are initially (time t_i) in the ground state of the He atom. Electron correlation is included as indicated by the dotted line. At time t_1 one of the two electrons leaves after the interaction with the field (denoted by '-x') so quickly that the second is *shaken-off* from the atom. The electrons propagate in the final state with momenta k_a and k_b in the presence of the field. The shake-off mechanism is well known for example from beta decay, where the nuclear charge is changed. It is also known to be one of the mechanisms for double ionization by absorption or Compton scattering of a

single photon (see the discussion in [33] and references therein). Its strong-field analog has been originally proposed by Fittinghoff *et al* [34].

Rescattering: In diagram 2(b) one electron becomes active first and absorbs energy from the field at time t_1, at a later time t_2 it interacts with the second electron via the electron–electron interaction and the two electrons may emerge together from the atom. During the time interval $t_2 - t_1$ the two electrons are in virtual intermediate states, namely one electron in the Volkov states (field dressed plane wave states) of momenta $\{k\}$ and the second electron in intermediate states of the ion $\{j\}$. The diagram includes the rather analogous *antenna* picture, advanced by Kuchiev [35–37], and the semi-classical *rescattering* mechanism proposed by Corkum [38] and Schafer *et al* [39]. According to the rescattering picture, first one electron is set free by quasi-static tunnelling. Then it is accelerated by the laser field, gains energy and, depending on the phase of the field upon the moment of ejection, the electron can be driven back to its parent ion when the field changes its sign. Upon recollision with the ion the electron can either recombine and emit higher harmonic radiation, scatter elastically and get further accelerated or it scatters inelastically with simultaneous excitation or ionization of the ion. Rescattering can be seen as a strong-field extension of the two-step-one mechanism (TS1), known for single photon double ionization at low photon energies [40]. In the TS1 mechanism, one electron absorbs the photon and knocks out the second one via an electron–electron collision on its way through the atom. Thus, while for the TS1 mechanism the electron correlation appears to be dominant on a very short time scale (a few attoseconds) and confined to a small region of space (the size of the electron cloud), in the rescattering mechanism there is a femtosecond time delay between the first and the second steps. The diagram in figure 2(b) involves in the intermediate state both, short-time propagation ($t_2 - t_1 < \pi/2\omega$, electron–electron collision on the way through the atom, TS1) and long-time propagation ($t_2 - t_1 > \pi/2\omega$, rescattering).

Collective tunnelling: According to this mechanism the two electrons tunnel out simultaneously from the atom or molecule. It was advanced by Eichmann *et al* [41] inspired by the fact that single ionization at sufficiently high field strengths is well described by a one-electron tunnelling formula (e.g. [42]). This mechanism is part of the *S*-matrix diagram in figure 2(c). Here, the two electrons interact independently, at times t_1 and t_2 respectively, with the field and leave the atom. The diagram includes the sequential double ionization for long intermediate time intervals $t_2 - t_1$ as well as a collective double ionization for short intermediate times.

The experimental observation that double ejection is strongly suppressed in ionization with circularly polarized light [43, 44] (see also figure 19 in [4]) provided strong evidence that the rescattering mechanism is dominantly responsible for double ionization by strong laser fields. The rescattering mechanism is inhibited by the circular polarization since the rotating electric field does not drive the electrons back to their parent ion. The other mechanisms, in contrast, are expected to be polarization independent.

Becker and Faisal have also identified [30, 31] in their IM*S*T analysis the rescattering diagram (figure 2(b)) as the dominant diagram for nonsequential double ionization. For example, its contribution to the total ionization rate was found to exceed by many orders of magnitude over that from the shake-off diagram [31]. It has been further shown by Zon [45] and Eichmann *et al* [41] that the rate of collective two-electron tunnelling is much too low to account for the large nonsequential double ionization yields. The strong dominance of the rescattering mechanism for the ejection of two electrons also suggests [23, 25] a physical mechanism for nonsequential multiple ionization, in which the first step of the process remains the same but the second is a generalization to an (e^-, ne^-) collisional ionization.

For the analysis of the ion yields of double and multiple ionization, Becker and Faisal proposed [24, 25, 46, 47] a simple model formula, which combines rates for single ionization
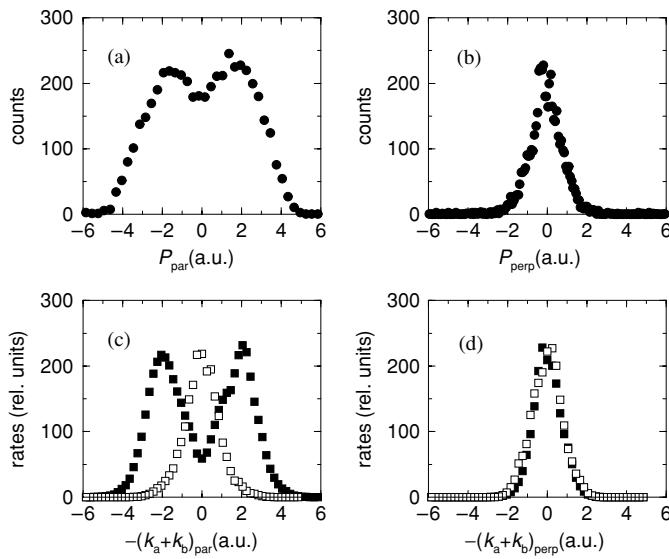
Figure 3. Distributions of the recoil momentum of doubly charged helium ions generated by 800 nm, 200 fs laser pulses at 6.6×10^{14} W cm^{-2}. Left-hand panels: components parallel to the field direction, right-hand panels: components perpendicular to the field direction. Experimental data (upper row, [55]) are compared with results of the S-matrix calculations [70] with (filled squares) and without (open squares) the final state Volkov dressing.

at the first stage of the process with collisional ionization rates $((e^-, ne^-), n = 2, 3, \ldots)$ at the second stage. Predictions of this model are found to be in good agreement with data of a large number of experiments [24, 25, 48]. As examples, the comparisons for the much discussed knee structure in double ionization of He at near infrared wavelengths and for the case of up to six-fold ionization of Xe as well as its absence at the UV wavelength are shown in figure 1 (solid lines). Before leaving this discussion of the total ion yields, we note that it has also been shown experimentally and theoretically [47] that electrons from an *inner shell* can be ejected through the mechanism of nonsequential double and multiple ionization.

3. Analysis of differential measurements

To gain further insight in the double ionization process, differential measurements which go beyond the measured total ion yields are necessary. For a long time, however, the experimental study of electron correlation has suffered from the technical challenge to observe more than one electron emerging from a multiple ionization event. Only recently a breakthrough has been made by two types of such experiments: electron time-of-flight measurements in coincidence with the ion charge state [49–53] and those using the COLTRIMS (cold target recoil ion momentum spectroscopy, [54]) technique, where the ion momentum alone [55–61] or in coincidence with the momentum of one of the electrons [62–69] has been measured.

3.1. Recoil ion momenta

Recoil ion momentum distributions have been measured for helium (He$^+$, He^{2+}) [55], neon (Ne$^+$ - Ne^{4+}) [56, 61] and argon (Ar^{1+} - Ar^{4+}) [64, 57, 61]. Figure 3 summarizes some of the experimental data for helium (upper row, [55]) in comparison with S-matrix results

(lower row, [70]) for 800 nm laser light at 6.6×10^{14} W cm^{-2}. Shown are the momentum components parallel (left-hand panels) and perpendicular (right-hand panels) to the field direction. The features of the distributions observed in the experiments are a distinct double peak structure for the parallel momentum component (figure 3(a)) and a single peak structure for the perpendicular component (figure 3(b)).

It has been shown [55, 56] that the double peak structure automatically rules out the shake-off [34] and the collective tunnelling [41] mechanisms, since for both a strong peak at the origin would be expected. At the same time, the peaks were found to be in qualitative agreement with the recollision [38] or the antenna [35] mechanism. As mentioned above, in the rescattering picture there is a significant time delay between the emission of the first electron and the return to its parent ion. Estimating $t_2 - t_1$ for a rescattering trajectory which has sufficient energy to ionize the residual ion leads to ion momenta close to the measured peak positions [55, 56, 58].

Soon after the measurement of the first ion momentum distributions, Becker and Faisal made the first theoretical predictions [70] for double ionization of He by evaluating the dominant Feynman diagram from the intense-field many-body S-matrix theory (cf figure 2(b)). The results for the momentum distributions of the He^{2+} ion calculated as the sum momentum of the two electrons are shown in figure 3(c), (d) (solid squares). The double peak structure, its width and the position of the maxima for the parallel component (panel c) are reproduced by the calculations as well as the single hump structure for the perpendicular component (panel d). The minimum at momentum zero in the distribution for the parallel momentum is more pronounced in the calculation than in the data, which might be due to non-negligible contributions from higher-order diagrams (see also discussion below). To unveil the physical origin responsible for the double hump structure, Becker and Faisal have evaluated the rescattering diagram also by replacing the final Volkov (or field dressed) states by plane waves. Physically, this corresponds to switching off the laser field after both electrons are in the continuum. In the calculation this leads to a collapse of the double peak structure to a single peak (open squares in figure 3(c)), which confirms the interpretation given above that it is the acceleration of the ion (or the electrons, respectively) in the field after the rescattering, which leads to the large ion momenta. The distribution perpendicular to field does not change (figure 3(d)), since the final state momenta of the electron do not couple to the field in this direction. It has been further shown by Jaroń and Becker [71] that the component of the sum-momentum parallel to the field is largest when the drift energy of the active electron in the intermediate state is close to zero.

The rescattering diagram has also been estimated by introducing different approximations in the evaluation. A stationary phase approximation has been used to evaluate the integrations over the time and the momentum in the intermediate state. This additional approximation reduces the computation time significantly and does not change the calculated ion momentum distribution significantly as shown by Goreslavskii and Popruzhenko (figure 4(c) [72, 73]). Kopold *et al* [74] further replaced the electron–electron interaction by a zero-range contact potential. Using these approximations they were able to show that a (third-order) diagram, which implies an excitation of the He$^+$ ion via the electron–electron interaction, followed by the ionization of the excited ion by the field, gives contributions near zero momentum of the recoil ion and may fill the valley in the parallel momentum distributions of the minimum at zero momentum.

A conceptionally different approach was used by Sacha and Eckhardt [75]. They argued that rescattering will produce a highly excited intermediate complex, which will then decay in the presence of the field. In a Wannier type analysis they studied the decay using classical trajectories in the saddle potential created by the field and the Coulomb potentials. Interestingly
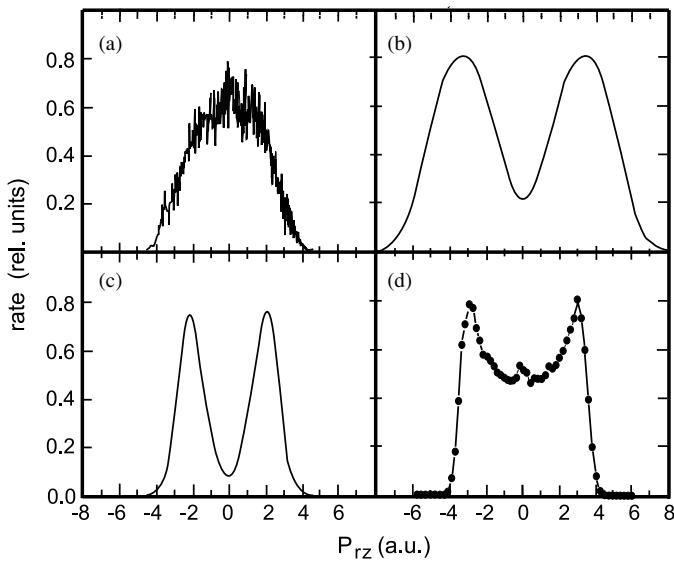
Figure 4. Momentum distributions of He^{2+} ions at an intensity of 6.6×10^{14} W cm^{-2} for all panels. p_{rz} is the component parallel to the laser polarization. (a) Solution of the one-dimensional Schrödinger equation [77], (b) classical trajectory Monte Carlo calculations [78], (c) S-matrix calculation with additional saddle point approximation [72] and (d) Wannier type calculation [75].

the recoil ion momentum exhibits a double peak structure that does not depend strongly on the time of creation but on the energy. Sacha and Eckhardt find parallel and perpendicular momentum distributions, which are for helium (figure 4(d)) and neon in reasonable agreement with the experiment. Recently, they extended this model to examine the decay of highly excited three electron atoms [76].

Computation of the time-dependent Schrödinger equation for two electrons in three dimensions is extremely challenging and there are no predictions of recoil ion momenta or other differential information in the 'long' wavelength regime of presently available high-intensity lasers up to now. Lein *et al* [77] reported the first results on recoil ion momenta based on an integration of the one-dimensional Schrödinger equation (see figure 4(a)). The momentum distribution peaks at zero momentum in contrast to all other results. This might be due to a well-known problem of one-dimensional calculations, namely that the effect of electron repulsion is overemphasized.

Chen *et al* [78] have performed a classical trajectory Monte Carlo calculation (CTMC) in which they solved the classical Hamilton equations of motion for all three particles in the field. The initial state in the simulation is determined by the momentum distributions following from tunnelling of one electron from the atom. The results of this calculation also yield the observed double peak structure (figure 4(b)).

Nevertheless, the interpretation remains puzzling, if one compares recoil ion momentum distributions for different targets. In figure 5 experimental data for the parallel component as obtained by de Jesus *et al* [60] for the doubly charged helium, neon and argon ions in 23 fs, linearly polarized Ti:sapphire laser pulses at intensities between 0.35×10^{15} W cm^{-2} and 1.25×10^{15} W cm^{-2} are shown. While the pronounced double peak structure along the polarization direction is found for the neon target at all intensities, this feature is considerably less apparent or even absent at the lowest intensity for the other two targets. Similar observations have been made for helium by Weber *et al* [55] and for neon by Eremina *et al* [65].
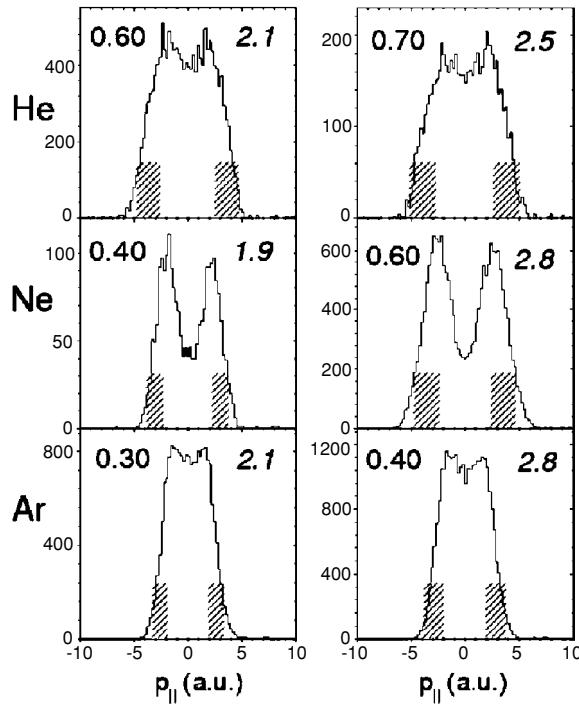
Figure 5. Longitudinal ion momentum distributions for double ionization of He, Ne and Ar at intensities as indicated in the upper left corner of each panel (in units of 10^{15} W cm^{-2}). Ratios of the maximum recollision impact energy to the ionization potential of the second electron, E_{rec}/I_p, are plotted in the upper right corners. The shaded areas represent the regions of the most probable momenta assuming classical electron motion and direct impact ionization.

According to the semi-classical rescattering model the final drift momentum distribution of the ion should depend on the ratio of the maximum recollision energy, E_{rec}, to the ionization potential of the second electron, I_p, only. Note that the data in figure 5 are taken at similar ratios of E_{rec}/I_p (indicated in the upper left corner of each panel). Obviously, the distributions show a strong target dependence.

An explanation for this observation has been put forward by de Jesus *et al* [60] based on the relative strength of the two mechanisms, namely the direct ionization of the second electron via rescattering and its excitation via rescattering followed by subsequent field ionization. In the latter mechanism ions with small momenta are generated. de Jesus *et al* have found that the contribution of the latter mechanism can exceed those of the former for He and Ar but not for Ne, which explains the differences between the measured recoil ion momentum distributions for the different targets (see figure 6). This is due to the fact that for He and Ar electron impact excitation cross sections for the singly charged ion exceed those for ionization at all energies, which is not the case for Ne. It will be interesting to see in future, if calculations based on one of the theories discussed above can further substantiate these conclusions.

Momentum distributions of triply and four-fold charged ions have been observed by Moshammer *et al* [56] for Ne^{3+} and by Rudenko *et al* [61] up to Ne^{4+} and Ar^{4+}. In figure 7, the results for the parallel momentum components observed in the latter experiment measured with 25 fs laser pulses at intensities of 1.2×10^{15} W cm^{-2} and 2×10^{15} W cm^{-2} are shown. The narrow distribution of the Ne^{2+} ions with a maximum at zero momentum indicates that
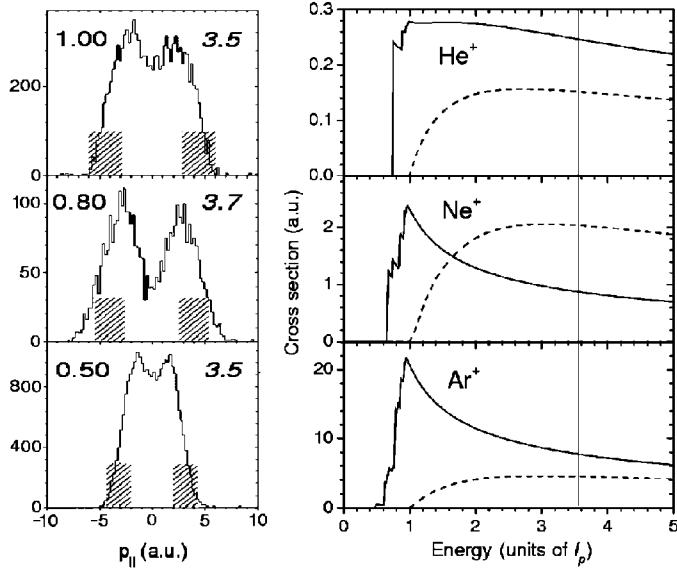
Figure 6. Left panel: ion momentum distributions as in figure 5 but for slightly higher intensities. Right panel: total excitation (solid lines) and ionization (dashed lines) cross sections of He^+, Ne^+ and Ar^+ as a function of the electron impact energy in units of the ionization potential. The vertical line indicates the maximum recollision energy for the present intensities.
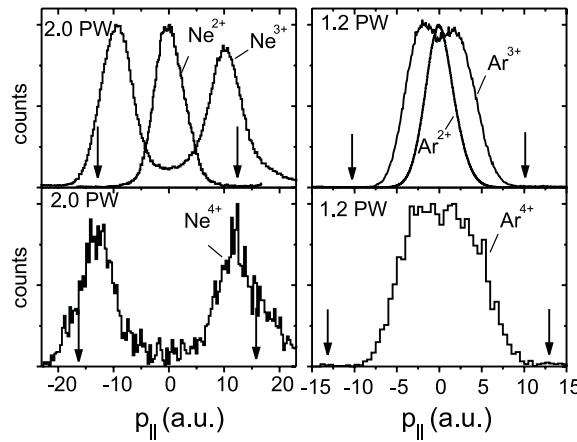
Figure 7. Longitudinal momentum distributions of the recoil ion for double-, triple- and four-fold ionization of Ne and Ar (see the text).

at the present intensities double ionization occurs via the sequential mechanism. At the same intensity the distributions for the higher charged states of Ne, however, exhibit a clear double peak structure with almost no ions created with zero momentum. The spectra extend slightly beyond $p_{max} = 2n\sqrt{U_p}$ ($n = 3, 4$) (indicated by the arrows), which corresponds to the maximum classical longitudinal momentum the Ne^{n+} ion gains when the electrons are set free via an (e, ne)-rescattering event. For the multiply charged Ar ions the distributions are very different. The Ar^{3+} distributions exhibit a shallow minimum at zero, whereas for the Ar^{4+} ions there is no double peak structure at all. Further, both the distributions are much narrower
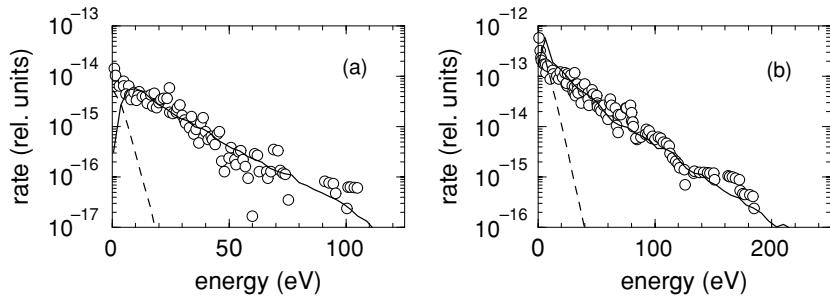
Figure 8. Electron energy spectra from double ionization of He at 780 nm and two intensities, (a) 4×10^{14} Wcm^{-2} and (b) 8×10^{14} W cm^{-2}. S-matrix results [31] from the rescattering diagram (solid lines) are compared with those from the shake-off diagram (dashed lines) and the experimental data (circles) obtained by Lafon *et al* [50].

than in the case of Ne and lie well within the classical limits of $2n\sqrt{U_p}$ (see arrows). This indicates that for Ar at these intensities the direct (e, ne)-rescattering event is not the dominant mechanism.

3.2. Electron energies

Electron energy distributions for double ionization have been reported for helium [50], argon [51, 53], neon [52] and xenon [49, 53]. A common feature of all these experiments is that the distributions generated via nonsequential double ionization extend to much larger energies than those generated in single ionization. Using the S-matrix theory Becker and Faisal have analysed [31] the data for He obtained by Lafon *et al* [50] at 780 nm. In figure 8, the results of calculations from the rescattering diagram (solid lines, cf figure 2(b)) and the shake-off diagram (dashed lines, cf figure 2(a)) are compared with the experimental data (circles) at (a) 4×10^{14} W cm^{-2} and (b) 8×10^{14} W cm^{-2}. In both, experiment and calculation, the emission direction of one electron has been fixed along the polarization direction while the energy and the emission direction of the other electron were kept unresolved (integrated in theory). It is seen from the comparison that the experimental data are in full agreement with the theoretical predictions from the rescattering diagram, except for a narrow region near the threshold. In contrast, the results for the shake-off diagram decrease very quickly and fail completely to follow the trend of the experimental data.

Recently, Chaloupka *et al* [53] have resolved distinct resonance-like structures in electron energy spectra of double ionization of Xe, while in Ar featureless spectra, consistent with the rescattering mechanism, have been observed. They interpreted this observation as a progression from the tunnelling and rescattering mechanism to an (unknown) multiphoton mechanism. There is no theoretical analysis of these observations up to now, and the underlying physics remains unclear.

3.3. Correlated electron momenta

More information can be obtained from the momentum correlation between the two electrons. In an experiment one possible choice would be to observe the momenta of both electrons in coincidence. In this case, the recoil ion momentum could be calculated from the momentum conservation. From an experimental point of view, however, it is easier to detect the ion and one of the electrons, in which case the momentum of the second electron can be inferred
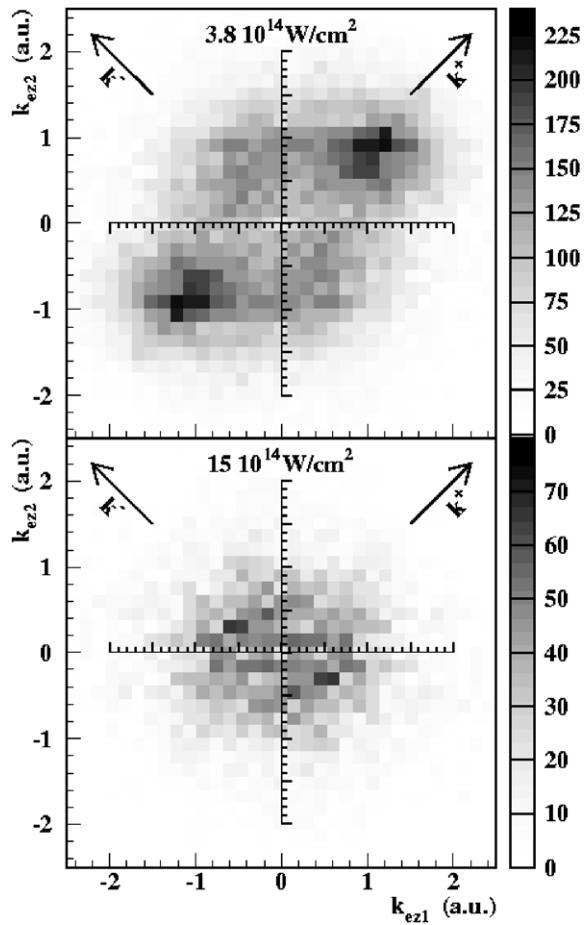
Figure 9. Momentum correlation between the two emitted electrons when an Ar^{2+} ion is produced in the focus of a 220 fs, 800 nm laser pulse at peak intensities of 3.8×10^{14} W cm^{-2} and 15×10^{14} W cm^{-2}. The horizontal axis shows the momentum component of one electron along the polarization of the laser field; the vertical axis represents the same momentum component of the corresponding second electron. Same sign of the momenta for both electrons represents an emission to the same half sphere. The data are integrated over the momentum components in the direction perpendicular to the polarization direction. The grey shading shows the differential rate in arbitrary units on a linear scale (adapted from [62]).

from momentum conservation. It is experimentally simpler, since the additional knowledge of the ion charge state allows for an effective suppression of random coincidences. Moreover, electron and ion are detected on opposite detectors circumventing possible problems of multihit detection. Many successful studies for single photon double ionization have been performed this way [33, 79–81].

Measurements of the momentum components parallel to the field of electron and ion while integrating over all the other momentum components have been reported by Weber *et al* [62], Feuerstein *et al* [64], Moshammer *et al* [68] and de Jesus *et al* [69]. The data of the first observations from double ionization of Ar are shown in figure 9 [62]. Events in the first and third quadrants are those where both electrons are emitted to the same hemisphere, the second and fourth quadrants correspond to emission to opposite half spheres. The upper panel
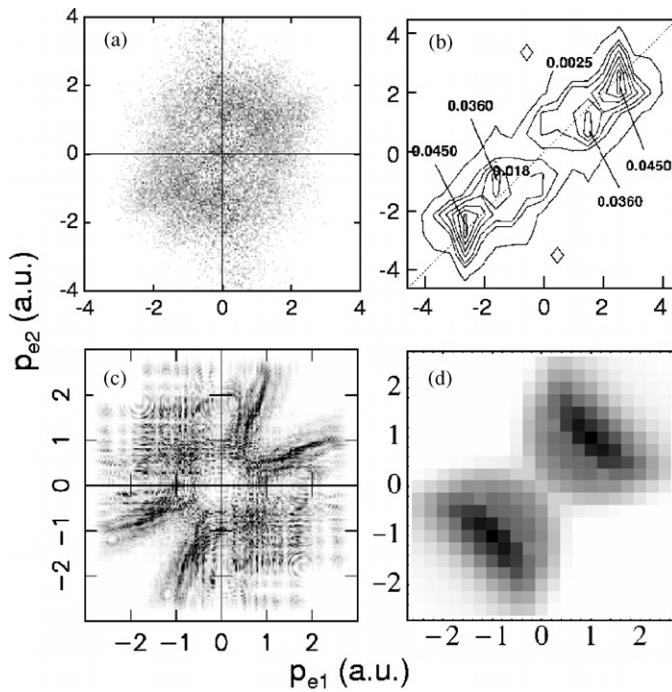
Figure 10. Components of the correlated momenta of the electrons parallel to the field direction for double ionization of He. (a) Experimental data at 5×10^{14} W cm^{-2} [69], (b) results from the classical trajectory Monte Carlo calculation at 10^{15} W cm^{-2} [78], (c) results of one-dimensional numerical simulations at 7×10^{14} W cm^{-2} [77] and (d) results from S-matrix calculations at 6.6×10^{14} W cm^{-2} [31].

shows the electron momenta at an intensity of 3.6×10^{14} W cm^{-2}, which is in the regime of nonsequential ionization. The distribution shows a strong correlation between the two electrons; they are most likely emitted to the same hemisphere with a similar momentum of about 1 au. At higher intensity, where double ionization proceeds sequentially this correlation is lost (lower panel in figure 9).

In figure 10(a) the correlated momenta of the two electrons parallel to the polarization direction for double ionization of helium by 23 fs, 5×10^{14} W cm^{-2}, as measured by de Jesus *et al* [69], are presented. Like argon [62, 64, 65], but different from neon [68], a considerable amount of events appears in the second and fourth quadrants. Thus, the correlated momentum spectra indicate that as for Ar (cf [64]) also for He another mechanism, different from direct ionization via rescattering, has to be present.

Also shown in figure 10 are theoretical predictions for the distribution of the electron momentum components parallel to the field direction at laser intensities close to the experimental one. First, the results from the CTMC calculation by Chen *et al* [78] are shown in panel (b). Although excitation of the ion due to rescattering is included in their calculations, a tunnelling ionization of the (excited) ion is excluded. Accordingly, the distribution of the final electron momenta is found to be well within the classically allowed regime (the first and third quadrants) for direct ionization by rescattering only. The results of a solution of the one-dimensional Schrödinger equation by Lein *et al* [77] (figure 10(c)) show, in agreement with the experimental data, a considerable flux in the second and fourth quadrants. However, discrepancies to the experimental results are obtained along the diagonal in the first and third
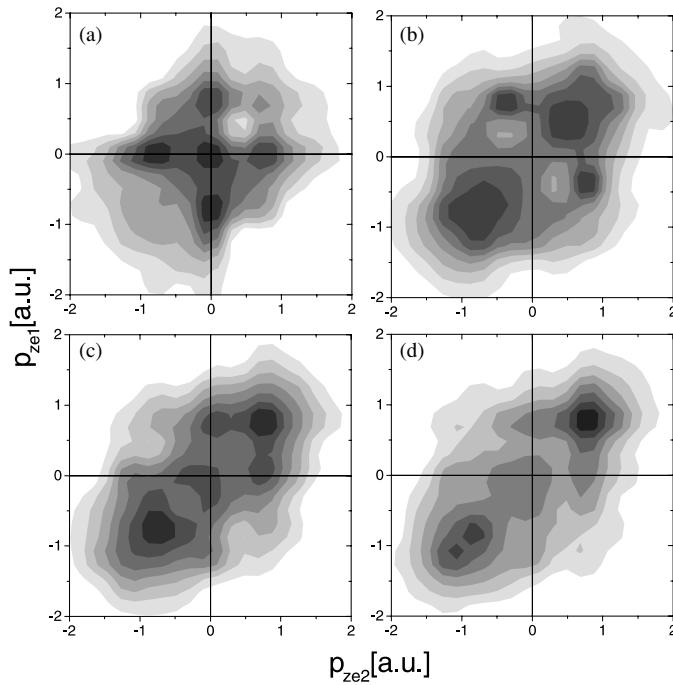
Figure 11. Momentum correlation between the two emitted electrons when an Ar^{2+} ion is produced in the focus of a 150 fs, 780 nm laser pulse at peak intensities of 4.7×10^{14} W cm^{-2}. Axis as in figure 9. Each panel represents a part of the final state for a fixed transverse momentum ($p_\perp$) of one of the electrons. (a) One of the electrons has a transverse momentum of $p_\perp < 0.1$ au, (b) $0.1 < p_\perp < 0.2$ au, (c) $0.2 < p_\perp < 0.3$ au, (d) $0.3 < p_\perp < 0.4$ au. The grey scale shows the differential rate in arbitrary units and linear scale (from [63]).

quadrants, when both electrons have the same longitudinal momentum. The maximum of the experimental distribution is located here with only a slight indication of a minimum along the diagonal, whereas a distinct minimum (zero) is found in the theory. Further calculations using the one-dimensional model Schrödinger equation by Haan *et al* [83–85] show similar results for the momentum distributions. This is obviously due to the restriction to a one-dimensional model, in which the electron–electron interaction is overestimated. Finally, panel (d) shows the results from the rescattering diagram of the *S*-matrix theory (cf figure 2(b)) obtained by Becker and Faisal [31]. Again, the distribution is overwhelmingly located in the first and third quadrants. Similar results have been obtained by other authors [82, 87, 88] calculating the rescattering diagram using additional approximations. This result underlines that the significant probabilities in the second and fourth quadrants go beyond the direct ionization by recollision. It would be interesting to see if the prediction [64] that an excitation of the ion upon recollision followed by ionization of the excited ion is responsible for these contributions can be substantiated by theoretical calculations. Experimentally this prediction has been supported by more complete experiments (see figure 13) which will be discussed below.

For double ionization of Ar, Weckenbrock *et al* [63] and Moshammer *et al* [86] measured in addition to the momentum parallel to the field also the transverse momentum of the detected electron. Both find that the longitudinal correlation pattern strongly depends on this transverse momentum (see figure 11). If one electron is emitted with any transverse momentum larger than 0.1 au (i.e. with some angle to the polarization axis) one mostly finds both electrons with
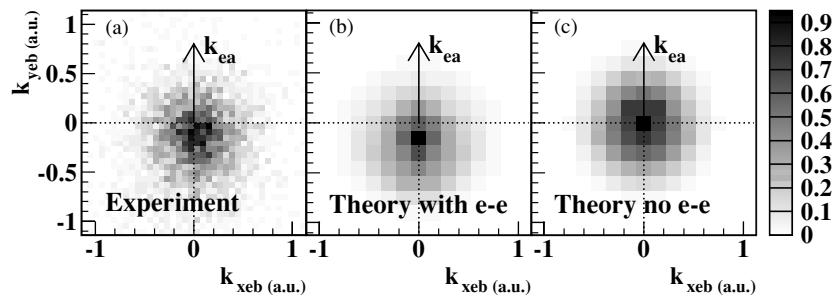
Figure 12. Momentum distribution of electron *b* in the plane perpendicular to the field direction for the double ionization of Ar at 780 nm and 1.9×10^{14} W cm^{-2} [66]. The perpendicular momentum direction of the other electron, *a*, is shown by the arrow. The data are integrated over all momentum components along the polarization direction and the magnitude of the momentum of electron *a*. A comparison is shown between (a) the experimental data, (b) theoretical results from the extended rescattering diagram including electron–electron interaction in the final state and (c) theoretical result from the rescattering diagram without electron–electron interaction in the final state.

a similar momentum component in the field direction. It is this configuration which dominates the integrated spectrum in figure 9. If, however, one electron is emitted almost parallel to the polarization with a very small transverse momentum of $p_\perp < 0.1$ au one finds that the parallel momentum distribution does no longer peak on the diagonal. In this case most likely one electron is fast and the other slow. It has been shown by Figueira de Morisson Faria *et al* [87, 88] by calculating the rescattering diagram using the stationary phase approximation and a zero-range potential that this is due to a strong electron–electron interaction between the two electrons in the final state.

Recently, Weckenbrock *et al* [66] investigated in a joint experimental and theoretical study the momentum balance in the direction perpendicular to the polarization axis. In this kinematical geometry the subtleties of the Coulombic interaction in the rescattering processes can be tested, since the perpendicular momentum components are not affected by the field. In figure 12, the distribution of the momentum components perpendicular to the polarization axis of one of the electrons, *b*, is plotted. The momentum component of the other electron in the same plane is shown by the arrow; the parallel components of both momenta as well as the magnitude of the momentum of electron *a* are not resolved in the experiment (integrated in the theory). The experimental data show clearly that the two electrons are emitted to opposite sides. This back-to-back emission is found to be due to a strong interaction between the two electrons after their double escape, as can be seen from the results of *S*-matrix calculations displayed in the other panels. Theoretical predictions and experimental data are in good agreement with each other (figure 12), when the rescattering diagram (figure 2(b)) is extended such that the full electron–electron interaction is taken into account in the final state (panel b). The results neglecting the electron–electron interaction (as in the original rescattering diagram, figure 2(b)) do not show the back-to-back characteristics (figure 12). This reveals the importance of the final-state repulsion between the electrons for the nonsequential double ionization process. In the experiment a back-to-back correlation between one of the electrons and the ion has also been observed. This could not be reproduced by the predictions from rescattering diagrams, which do not include effects of the electron–ion interaction and the collisional excitation process.

Kinematically complete experiments, i.e. experiments in which all momentum components of all particles are detected, have been reported by Weckenbrock *et al* [89]
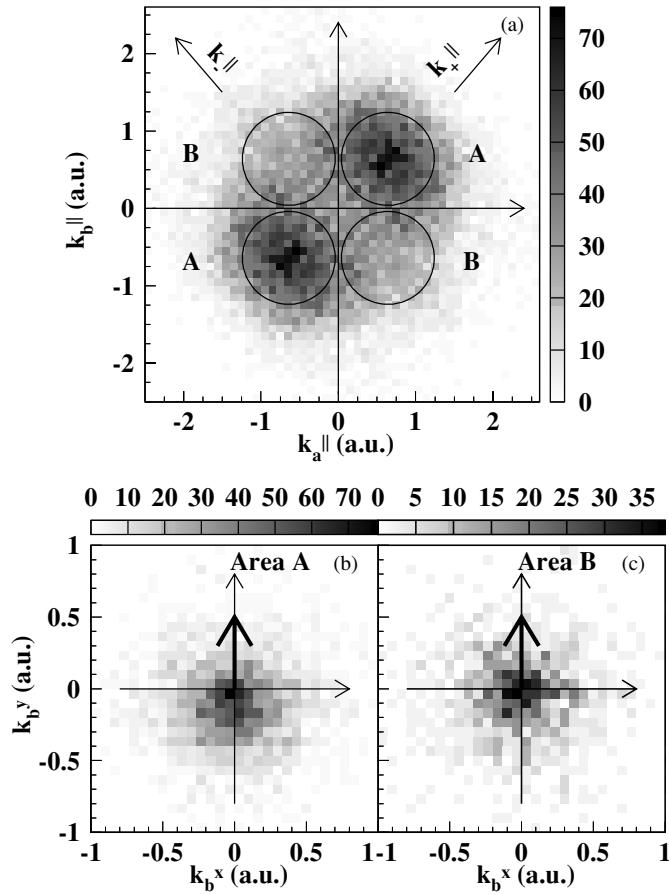
Figure 13. Double ionization of neon at 1.9×10^{14} W cm^{-2}, 800 nm, 40 fs. (a) horizontal axis: momentum of electron a parallel to the polarization direction, vertical axis: momentum of electron b parallel to the polarization direction. The areas indicated by the circles show the region of events selected in panels (b) and (c). (b) Momentum components of electron b in the plane perpendicular to the polarization, the perpendicular momentum of electron a is along the positive y axis as shown by the arrow. Only events within the circles in region A have been selected. (c) same as (b) but for events in circles in region B (from [89]).

for double ionization of neon when the recollision energy of the first electron is on the order of the ionization potential. The experiment finds that the electron repulsion in the perpendicular plane (as for example in figure 12) is only present if both electrons have similar longitudinal momenta (figure 13). In contrast, repulsion is not visible for events where the two electrons are located in the second and fourth quadrants (figure 13(a)), i.e. are driven by the field in opposite direction. These findings directly support the interpretation of parallel momenta as time stamps which we put forward throughout this paper Correlated electron momentum detection is a subcycle time correlation measurement on the attosecond time scale. For the case when the recolliding electron is close to the ionization threshold, which is well fulfilled in the experiment shown in figure 13, the difference in the parallel momenta between the electrons corresponds to the difference of their time of birth. Electrons in regions A (figure 13(a)) are both created at the time of recollision while electrons in region B are emitted at different times. In consequence, electrons in region A show repulsions in the perpendicular plane while those
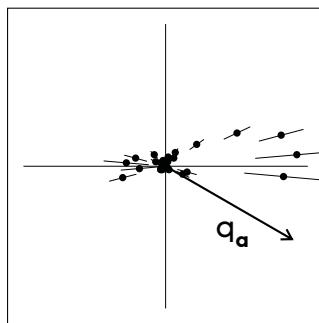
Figure 14. Double ionization of neon at 1.9×10^{14} W cm^{-2}, 800 nm, 40 fs. Angular distribution of electron b. The polarization axis is horizontal, the sum energy of electrons a and b is 10 eV $< (E_a + E_b) < 24$ eV. Both electrons have the same energy (from [89]).

in region B do not feel their repulsion. The latter electrons are likely produced via recollision with excitation followed by delayed field ionization as discussed above.

The final step towards complete information on the strong field double ionization process is to investigate the angular distribution of one electron of well-defined energy for fixed angle and energy of the second electron. First successful steps towards this goal have also been done for the multiphoton case [89]. Figure 14 shows one of those angular distributions, which highlight that most of the electrons are emitted with only a small angle between them with some influence of the electron repulsion still visible. There is, however, a smaller second lobe of electrons which are emitted back to back. Once such studies are performed with an energy resolution on the electron sum energy below the single photon energy, it can be expected that dipole selection rules become visible in these distributions as they dominate the structure of the three-particle continuum for the single photon case.

4. Outlook

In the future, we will certainly experience a continuation of the rapid progress on both sides, the COLTRIMS technique and in laser technology, and theoretical efforts towards *ab initio* simulations and many-electron emission. For the laser technology, efforts concentrate to produce ultrashort pulses with only two or three optical cycles as well as to control the phase of the carrier wave within the pulse envelope over reasonably long time scales (e.g. [90]) and to generate sub-fs pulses (e.g. [91, 92]). With such pulses it will be possible not only to precisely adjust the temporal shape of the electric field of the light wave but also to control its direction and strength at the instant of electron recollision. It can be anticipated that this will enable new insights into the many aspects of the electron dynamics in double ionization on fs or even sub-fs time scales. Pioneering measurements for single ionization [93–95] and, very recently, theoretical predictions [96] and observations [97] for double ionization have already indicated a strong dependence of the electron emission characteristics on the carrier-envelope phase. On the experimental side, though kinematically complete data sets on double ionization of Ne have been collected for the first time, further experiments with improved statistics are certainly needed to ultimately test theory and to disentangle the still unexplained target dependences. Clearly, most desirable are fully differential data with good resolution for double ionization of He, the prototype system for theory. With the advent of larger computer systems, one can anticipate that *ab initio* simulations of this simplest two-electron system interacting with infrared laser pulses

will become available in the coming years. This will further help in unveiling the temporal details of the mechanism leading to nonsequential double ionization and may also lead to improved models for multiple ionization. Concerning triple or even quadruple ionization, so far only the ion momenta have been measured for Ar and Ne. In order to obtain conclusive answers about the involved reaction pathways as well as on their dependences on the target structure measurements differential in the electron momenta represent most likely the next step.

Another important future direction is the study of the wavelength dependence of double ionization. At present, experimental data are at hand only for the two extreme cases, namely single and multiphoton absorption (more than 50 photons for the case of He). The intermediate regime of two or three photon two-electron transitions is experimentally completely unexplored. This will change in the very near future when the free-electron laser at the TESLA Test facility in Hamburg starts its operation in the beginning of 2005. It will open exciting possibilities to explore a new regime of nonlinear multi-photon processes, where only a few high-energy photons interact with few electrons. Experiments for two-photon double ionization of helium are under preparation. Theoretical investigations in this direction have already begun.

Acknowledgments

References

[1] Einstein A 1905 *Ann. Phys., Lpz.* **17** 132
[2] Göppert-Mayer M 1931 *Ann. Phys., Lpz.* **9** 273
[3] Burnett K, Reed V and Knight P 1993 *J. Phys. B: At. Mol. Opt. Phys.* **26** 561
[4] DiMauro L F and Agostini P 1995 *Adv. At. Mol. Opt. Phys.* **35** 79
[5] Protopapas M, Keitel C and Knight P 1997 *Rep. Prog. Phys.* **60** 389
[6] Ehlotzky F, Jaroń A and Kamiński J 1998 *Phys. Rep.* **297** 63
[7] Joachain C J, Dörr M and Kylstra N J 2000 *Adv. At. Mol. Opt. Phys.* **42** 225
[8] Ehlotzky F 2001 *Phys. Rep.* **345** 175
[9] Becker W, Grasbon F, Kopold R, Milosevic D B, Paulus G G and Walther H 2002 *Adv. At. Mol. Opt. Phys.* **48** 35
[10] Milosevic D B and Ehlotzky F 2003 *Adv. At. Mol. Opt. Phys.* **49** 373
[11] McGuire J 1997 *Electron Correlation Dynamics in Atomic Collisions* (Cambridge: Cambridge University Press)
[12] Briggs J and Schmidt V 2000 *J. Phys. B: At. Mol. Opt. Phys.* **33** R1

[13] Doerner R, Schmidt-Böcking H, Weber Th, Jahnke T, Schöffler M, Knapp A, Hattass M, Czasch A, Schmidt L Ph H and Jagutzki O 2003 *Radint. Phys. Chem.* **70** 191

[14] Parker J, Taylor K T, Clark C W and Blodgett-Ford S 1996 *J. Phys. B: At. Mol. Opt. Phys.* **29** L33

[15] Dundas D, Taylor K, Parker J and Smyth E 1999 *J. Phys. B: At. Mol. Opt. Phys.* **32** L231

[16] Taylor K, Parker J, Dundas D, Smyth E and Vitirito S 1999 *Laser Phys.* **9** 98

[17] Parker J S, Moore L R, Dundas D and Taylor K T 2000 *J. Phys. B: At. Mol. Opt. Phys.* **33** L691

[18] Parker J S, Moore L R, Meharg K J, Dundas D and Taylor K T 2001 *J. Phys. B: At. Mol. Opt. Phys.* **34** L69

[19] Parker J, Doherty B J S, Meharg K J and Taylor K T 2003 *J. Phys. B: At. Mol. Opt. Phys.* **36** L393

[20] Kulander K C 1988 *Phys. Rev.* A **38** 778

[21] Walker B, Sheehy B, DiMauro L F, Agostini P, Schafer K J and Kulander K C 1994 *Phys. Rev. Lett.* **73** 1227

[22] Charalambidis D, Xenakis D, Uiterwaal C J G J, Zhang J, Schröder H, Faucher O and Lambropoulos P 1997 *J. Phys. B: At. Mol. Opt. Phys.* **30** 1467

[23] Larochelle S, Talebpour A and Chin S L 1998 *J. Phys. B: At. Mol. Opt. Phys.* **31** 1215

[24] Becker A and Faisal F H M 1999 *Phys. Rev.* A **59** R1742

[25] Becker A and Faisal F H M 1999 *Phys. Rev.* A **59** R3182

[26] L'Huillier A, Lompre L A, Mainfray G and Manus C 1982 *Phys. Rev. Lett.* **48** 1814

[27] Hino K, Ishihara T, Shimizu F, Toshima N and McGuire J H 1993 *Phys. Rev.* A **48** 1271

[28] Kheifets A, Bray I, Soejima K, Danjo A, Okuno K and Yagishita A 2001 *J. Phys. B: At. Mol. Opt. Phys.* **34** L247

[29] Faisal F H M and Becker A *Selected Topics on Electron Physics* (New York: Plenum) p 397

[30] Becker A and Faisal F H M 1996 *J. Phys. B: At. Mol. Opt. Phys.* **29** L197

[31] Becker A and Faisal F H M 2002 *Phys. Rev. Lett.* **89** 193003

[32] Becker A and Faisal F H M 2005 *J. Phys. B: At. Mol. Opt. Phys.* **38** R1

[33] Dörner R, Bräuning H, Feagin J, Mergel V, Jagutzki O, Spielberger L, Vogt T, Khemliche H, Prior M and Ullrich J 1998 *Phys. Rev.* A **57** 1074

[34] Fittinghoff D N, Bolton P R, Chang B and Kulander K C 1992 *Phys. Rev. Lett.* **69** 2642

[35] Kuchiev M Y 1987 *Sov. Phys.—JETP Lett.* **45** 404

[36] Kuchiev M Y 1995 *J. Phys. B: At. Mol. Opt. Phys.* **28** 5093

[37] Kuchiev M Y 1995 *Phys. Lett.* A **212** 77

[38] Corkum P 1993 *Phys. Rev. Lett.* **71** 1994

[39] Schafer K, Yang B, DiMauro L and Kulander K 1993 *Phys. Rev. Lett.* **70** 1599

[40] Samson J 1990 *Phys. Rev. Lett.* **65** 2863

[41] Eichmann U, Dörr M, Maeda H, Becker W and Sandner W 2000 *Phys. Rev. Lett.* **84** 3550

[42] Keldysh L V 1965 *Sov. Phys.—JETP* **20** 1307

[43] Fittinghoff D, Bolton P, Chang B and Kulander K 1994 *Phys. Rev.* A **49** 2174

[44] Dietrich P, Burnett N H, Ivanov M and Corkum P B 1994 *Phys. Rev.* A **50** R3585

[45] Zon B 1999 *Sov. Phys.—JETP* **89** 219

[46] Becker A and Faisal F H M 1999 *J. Phys. B: At. Mol. Opt. Phys.* **32** L335

[47] Becker A, Faisal F H M, Liang Y, Augst S, Beaudoin Y, Chaker M and Chin S L 2000 *J. Phys. B: At. Mol. Opt. Phys.* **33** L547

[48] Maeda H, Dammasch M, Eichmann U, Sandner W, Becker A and Faisal F H M 2000 *Phys. Rev.* A **62** 035402

[49] Witzel B, Papadogiannis N A and Charalambidis D 2000 *Phys. Rev. Lett.* **85** 2268

[50] Lafon R, Chaloupka J L, Sheehy B, Paul P M, Agostini P, Kulander K C and DiMauro L F 2001 *Phys. Rev. Lett.* **86** 2762

[51] Peterson E and Bucksbaum P 2001 *Phys. Rev.* A **64** 053405

[52] Moshammer R, Feuerstein B, Fischer D, Dorn A, Schröter C, Deipenwisch J, Lopez-Urrutia J, Höhr C, Neumayer P and Ullrich J 2001 *Opt. Express* **8** 358

[53] Chaloupka J L, Rudati J, Lafon R, Agostini P, Kulander K C and DiMauro L F 2003 *Phys. Rev. Lett.* **90** 033002

[54] Ullrich J, Moshammer R, Dorn A, Dörner R, Schmidt L Ph and Schmidt-Böcking H 2003 *Rep. Prog. Phys.* **66** 1463

[55] Weber T, Weckenbrock M, Staudte A, Spielberger L, Jagutzki O, Mergel V, Urbasch G, Vollmer M, Giessen H and Dörner R 2000 *Phys. Rev. Lett.* **84** 443

[56] Moshammer R, Feuerstein B, Schmitt W, Dorn A, Schröter C, Ullrich J, Rottke H, Trump C, Wittmann M and Korn G 2000 *Phys. Rev. Lett.* **84** 447

[57] Weber T, Weckenbrock M, Staudte A, Spielberger L, Jagutzki O, Mergel V, Urbasch G, Vollmer M, Giessen H and Dörner R 2000 *J. Phys. B: At. Mol. Opt. Phys.* **33** L127

[58] Feuerstein B, Moshammer R and Ullrich J 2000 *J. Phys. B: At. Mol. Opt. Phys.* **33** L823

[59] Weber T, Jagutzki O, Hattass M, Staudte A, Nauert A, Schmidt L, Prior M, Landers A, Bräuning-Demian A and Bräuning H 2001 *J. Phys. B: At. Mol. Opt. Phys.* **34** 3669

[60] de Jesus V L B, Feuerstein B, Zrost K, Fischer D, Rudenko A, Afaneh F, Schröter C D, Moshammer R and Ullrich J 2004 *J. Phys. B: At. Mol. Opt. Phys.* **37** L161

[61] Rudenko A, Zrost K, Schröter C D, de Jesus V L B, Feuerstein B, Moshammer R and Ullrich J 2004 *Phys. Rev. Lett.* **93** 253001

[62] Weber T, Giessen H, Weckenbrock M, Staudte A, Spielberger L, Jagutzki O, Mergel V, Urbasch G, Vollmer M and Dörner R 2000 *Nature* **404** 608

[63] Weckenbrock M, Hattass M, Czasch A, Jagutzki O, Schmidt L, Weber T, Roskos H, Löffler T, Thomson M and Dörner R 2001 *J. Phys. B: At. Mol. Opt. Phys.* **34** L449

[64] Feuerstein B, Moshammer R, Fischer D, Dorn A, Schröter C D, Deipenwisch J, Lopez-Urrutia J, Höhr C, Neumayer P and Ullrich J 2001 *Phys. Rev. Lett.* **87** 043003

[65] Eremina E *et al* 2003 *J. Phys. B: At. Mol. Opt. Phys.* **36** 3269

[66] Weckenbrock M, Becker A, Staudte A, Kammer S, Smolarski M, Bhardwaj V R, Rajner D M, Villeneuve D M, Corkum P B and Dörner R 2003 *Phys. Rev. Lett.* **91** 123004

[67] Weckenbrock M *et al* 2003 *Phys. Rev. Lett.* **91** 123004

[68] Moshammer R *et al* 2003 *J. Phys. B: At. Mol. Opt. Phys.* **36** L113

[69] de Jesus V L B, Rudenko A, Feuerstein B, Zrost K, Schröter C D, Moshammer R and Ullrich J 2004 *J. Electron. Spectrosc.* **141** 127

[70] Becker A and Faisal F H M 2000 *Phys. Rev. Lett.* **84** 3546

[71] Jaroń A and Becker A 2003 *Phys. Rev.* A **67** 035401

[72] Goreslavskii S and Popruzhenko S 2001 *Opt. Express* **8** 395

[73] Goreslavskii S and Popruzhenko S 2001 *J. Phys. B: At. Mol. Opt. Phys.* **34** L239

[74] Kopold R, Becker W, Rottke H and Sandner W 2000 *Phys. Rev. Lett.* **85** 3781

[75] Sacha K and Eckhardt B 2001 *Phys. Rev.* A **63** 043414

[76] Sacha K and Eckhardt B 2001 *Phys. Rev.* A **64** 053401

[77] Lein M, Gross E and Engel V 2000 *Phys. Rev. Lett.* **85** 4707

[78] Chen J, Liu J, Fu L and Zheng W 2000 *Phys. Rev.* A **63** 011404(R)

[79] Dörner R, Feagin J, Cocke C, Bräuning H, Jagutzki O, Jung M, Kanter E, Khemliche H, Kravis S and Mergel V 1996 *Phys. Rev. Lett.* **77** 1024
     Dörner R, Feagin J, Cocke C, Bräuning H, Jagutzki O, Jung M, Kanter E, Khemliche H, Kravis S and Mergel V 1997 *Phys. Rev. Lett.* **78** 2031

[80] Mergel V, Achler M, Dörner R, Khayyat K, Kambara T, Awaya Y, Zoran V, Nyström B, Spielberger L and McGuire J 1998 *Phys. Rev. Lett.* **80** 5301

[81] Achler M, Mergel V, Spielberger L, Dörner Y A R and Schmidt-Böcking H 2001 *J. Phys. B: At. Mol. Opt. Phys.* **34** 965

[82] Goreslavskii S, Popruzhenko S, Kopold R and Becker W 2001 *Phys. Rev.* A **64** 053402

[83] Panfili R, Haan S L and Eberly J H 2002 *Phys. Rev. Lett.* **89** 113001

[84] Haan S L, Wheeler P S, Panfili R and Eberly J H 2002 *Phys. Rev.* A **66** 061402

[85] Haan S L, Cully J C and Hoekema K 2004 *Opt. Express* **12** 4758

[86] Moshammer R *et al* 2002 *Phys. Rev.* A **65** 035401

[87] Figueria de Morisson Faria C, Liu X, Becker W and Schomerus H 2004 *Phys. Rev.* A **69** 021402(R)

[88] Figueria de Morisson Faria C, Schomerus H, Liu X and Becker W 2004 *Phys. Rev.* A **69** 043405

[89] Weckenbrock M *et al* 2004 *Phys. Rev. Lett.* **92** 213002

[90] Baltuska A, Udem T, Uiberacker M, Hentschel M, Goulielmakis E, Gohle C, Yakovlev V S, Scrinzi A, Hänsch T W and Krausz F 2003 *Nature* **421** 611

[91] Hentschel M, Kienberger R, Spielmann Ch, Reider G A, Milosevic N, Brabec T, Corkum P B, Heinzmann U, Drescher M and Krausz F 2001 *Nature* **414** 509

[92] Paul P M, Toma E S, Breger P, Mullot G, Augé G, Balcou Ph, Muller H G and Agostini P 2001 *Science* **292** 1689

[93] Paulus G G, Grasbon F, Walther H, Villoresi P, Nisoli M, Stagira S, Priori E and De Silvestri S 2001 *Nature* **414** 182

[94] Paulus G G, Lindner F, Walther H, Baltuska A, Goulielmakis E, Lezius M and Krausz F 2003 *Phys. Rev. Lett.* **91** 253004

[95] Lindner F, Paulus G G, Walther H, Baltuska A, Goulielmakis E, Lezius M and Krausz F 2004 *Phys. Rev. Lett.* **92** 113001

[96] Liu X and Figueira de Morisson Faria C 2004 *Phys. Rev. Lett.* **92** 133006

[97] Liu X *et al* 2004 *Phys. Rev. Lett.* **93** 263001